# New monitoring technologies in mechanical systems

Aldo Sestieri[1,2], Antonio Carcaterra[1,2], Nicola Roveri[1,2]

[1]Department of Mechanical and Aerospace Engineering, Sapienza University of Rome, via Eudossiana 18, 00184 Rome, Italy
[2]CNIS- Center of Nanotechnology Sapienza, Rome, Italy
{Aldo.Sestieri, Antonio.Carcaterra, Nicola.Roveri}@uniroma1.it}

## Abstract

The actual capability of monitoring mechanical systems is based on new generation of sensors, modeling and algorithms for the detection of properties, operating conditions and/or failures of the monitored system. The present paper, on the basis of several projects in progress at the University La Sapienza, Rome, illustrates the combination of new sensing technologies and signal processing techniques of the acquired data, based on appropriate modeling of the monitored system. Particular emphasis is given to optical sensors and their application to keep under control special mechanical components as railways, viaducts, tires, and to the development of new measurement devices based on fluid-structure interaction.

## 1 Introduction

This paper proposes new technologies for monitoring mechanical systems and civil structures. More specifically monitoring and damage detection of structures, monitoring of mechanical contacts, identification of flow speed based on optical sensors have been developed and used recently in several applications. These activities are carried on at La Sapienza University Labs, namely in the Department of Mechanical and Aerospace Engineering and in the Nanotechnology Center – CNIS, Rome.

Some of the studied applications are aimed to shape monitoring, as those referred to sailing boat musts and airplane wings with the final goal of controlling their deflection for performance efficiency; others have diagnostic purposes, as topics on train rails, motorway viaducts, high speed boat drones and engines; others, finally, are devoted to control mechanical systems, specifically studies addressed to car suspensions and tires, with emphasis to experimental investigation of rolling phenomena, structural health and grip. Each of these applications require of course appropriate sensors, efficient modeling of the considered system and specific hardware and software to obtain the expected goals in a global process, here called **monitoring technology** of the system **S**.

Philosophically speaking, when addressing a particular engineering problem in the general context stated before, we define an **identification goal**. It is supposed that we have in mind or can develop some specific **algorithms** or procedures that can help to reach that goal, with the support of an appropriate set of measurements on a limited part of the system and a limited set of physical variables observed by dedicated **sensors**.

More precisely, $V_k(x_j)$ represents the physical variables $V_k$, $k=1,2,...M$, measured at points $x_j$, $j=1,2,...N$. The whole system **S** is identified by a finite set of *M* variables $\{V_k(X)\}$ defined over a continuous domain **X**. In general, the monitoring system uses a set of M'< M variables, accessible only over a limited subset of points $\{x_j\}\in\mathbf{X}$. Let us call the set $\{V_k(x_j)\}$ ($k=1,2,...M'$) the monitored system $\mathbf{S}_m$, complementary to the unmonitored system $\mathbf{S}_u$, that contains the information of interest to reach the required goal, such that $\mathbf{S}\equiv\mathbf{S}_m\cup\mathbf{S}_u$. Very often, some **model** of the system should be part of the monitoring process. In fact, the model consists frequently of an operator **L** (differential, integral or of different nature) such that $\mathbf{L}\left[V_k(x)\right]=0$. This equation permits to correlate implicitly $\mathbf{S}_m$ to $\mathbf{S}_u$: the procedure used to extract $\mathbf{S}_u$ form the previous equation is the **identification algorithm**.

Such elements, the goal, the sensors, the model and the algorithm are strictly interrelated with one another: to reach a particular goal we may follow different options, each one related to some method and requiring some knowledge of the system that in general can be obtained by appropriate measurements or/and appropriate description of the system. Once this information is available, the resulting data must be subsequently processed to obtain the expected goal. Sometimes only the experimental information can be sufficient, without the need of a system modeling, especially when the goal involves a simple data processing, but whenever the problem becomes more complex, some information on the system itself can be useful or strictly necessary.

The algorithm can involve either simple or sophisticated data processing or require the development of techniques focused to manipulate such data and obtain the necessary result.

Thus, the monitoring technology is made of different dowels that, in function of the engineering applications, may have different contents. With reference to the applications cited above, we will describe in the following few examples, related to trains, tires and related infrastructures as viaducts, bridges and railways, showing how the three dowels of the monitoring technology, sensors, modelling and signal processing, play together when applied to real systems of industrial interest, and present some significant engineering results.

# 2 Localized damage detection on road viaducts and bridges.

So far, this piece of work was theoretically developed and tested on a beam model. The technique is able to identify presence and location of a damage along the beam due to a travelling load, as well as the load characteristics, such as the mass and speed, for stationary and time-dependent systems. The measured data are processed by the Hilbert-Huang technique [1]. The identification capabilities of the proposed techniques are studied by varying the damage locations, crack depths and load characteristics [2]. The effect of ambient noise is also taken into account. Theoretical and numerical results show that the proposed method is rather accurate: the results are not very sensitive to the crack depth and ambient noise, while they are sensibly affected by the damage location and by the speed of the moving load. The theoretical analysis identifies a characteristic load velocity interval, depending on both the first natural frequency of the beam and the damage location, within which the HHT can be successfully applied.

## 2.1 Modeling

The use of vibration measurements for structural health monitoring has been applied in many engineering fields during the last three decades [3]. Nearly all the developed data-processing techniques depend strongly on the loading conditions and the experimental setup. Generally, a typical experimental setup relies on the acquisition, from multiple measurement points, of free or forced vibrations, purposely excited by a known, controllable, force. However, it is very difficult, costly and time consuming to generate the data in this way for real civil structures. Moreover only a few measurement points are usually available.

A very attractive and challenging field of research is related to the use of the forced response under ambient loads, such as vehicular traffic. There are indeed several connected problems: (i) loading conditions are not often controllable, (ii) the signal to noise ratio is highly affected by the moving load mass (the lighter the weight the poorer the signal), (iii) ambient load often produces nonstationary and nonlinear signals, (iv) massive travelling loads are often characterized by low frequencies, narrow bandwidth spectra, and are not able to excite wavelengths comparable with the characteristic dimension of the damage. The forced response of intact or slightly damaged civil structures is generally approximated by linear models. As the severity of the damage increases, structures exhibit a nonlinear behavior, especially when the moving load crosses the damaged section. Conventional techniques are not suited for analyzing such cases [4-9]. In fact, in real applications the characteristic of the load are not easy amenable of monitoring, and an output-only identification approach should be adopted. Here the focus is addressed to forced excitations generated by moving loads, producing nonstationary responses and time-varying modal parameters, that received significant attention in the last years [10-13].

To overcome the mentioned problems, in 1998 Huang et al. [1] developed an innovative time-frequency technique, known as Hilbert–Huang transform (HHT), able to analyze nonlinear systems and/or nonstationary data. Its core relies on the so-called Empirical Mode Decomposition (EMD), which permits to decompose the acquired signal into a set of basis functions, called Implicit Mode Functions (IMFs). They describe the vibratory response of the system and are a complete, adaptive and nearly orthogonal representation of the analyzed signal. Each IMF is almost mono-component [1], thus the implicit mode function family can determine all the instantaneous frequencies of the nonstationary signal, even from nonlinear structures [1]. The IMFs are processed through the Hilbert transform, to obtain the Hilbert spectrum of the signal, which enlightens unique features of the analyzed data.

In [2], the damaged structure is modeled as a two-span beam, each span obeying the Euler-Bernoulli beam theory, and the crack is modeled as an equivalent torsional spring (figure 1).

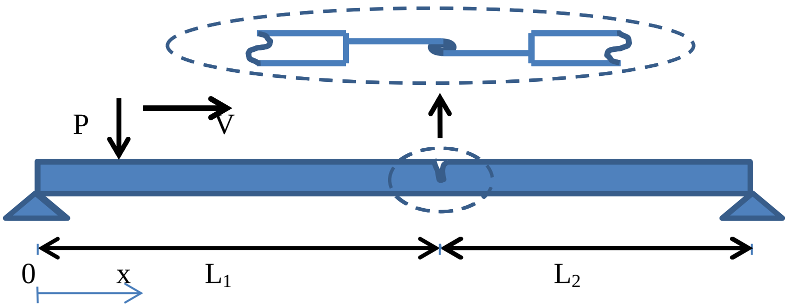


Figure 1: Modeling of the beam and the crack

Using the analytical transfer matrix method, analytical mode shape functions are calculated. The forced response is then obtained by modal analysis or by numerical integration of the time-variant equations of motion and the single-point responses are processed by the Hilbert-Huang transform, from which the instantaneous frequencies are extracted. The damage location is revealed by the inspection of the first instantaneous frequency (IF) curve, which presents a sharp crest in correspondence of the damaged section. In case of time-varying systems, an optimization algorithm, based on the comparison between the first IF and the analytical approximation of the first natural frequency, allows the estimation of the mass and the speed of the moving load. The effect of the moving load is then filtered out from the IF and the damage location is identified. The capabilities of the proposed technique are studied varying the load, the damage characteristics and the effect of the ambient noise.

### 2.2 Numerical validation and discussion

To evaluate the performance of the proposed technique, on the detection of damage in bridge structures, some numerical examples are presented. The aim is to evaluate the sensitivity of the method to:

- the crack depth $d$;
- the crack location $L_1$;
- the velocity of the moving load $V$;
- the ambient noise.

All the following examples consider a simply supported beam, whose physical-geometric parameters are: modulus of elasticity $E = 2.00 \cdot 10^{11}$ N/m$^2$, material density $\rho = 7800$ Kg/m$^3$, beam length $L$=20 m, cross section height and width $h$=$b$=0.2 m; the modulus of the load is $|P| = 1000$ N (downwards oriented). The crack position and depth are chosen as follow: $L_1 = 0.4L$ and $d = 0.4h$, respectively, and the speed of the moving load is $V$=2.8 m/s (10 km/h).

The first plot in figure 2 shows the nondimensional forced response corrupted with 10% noise level. The second plot in figure 2 shows the FFT of the signal. The Fourier transform captures the frequency shift of the fundamental frequency due to the damage (1.6% smaller than the undamaged case), but cannot locate it. Figure 3 shows the first IF curve, evaluated for 0%, 5% and 10% noise levels. Even if the noise introduces a modulation in the instantaneous frequency plots, the damage position is still correctly identified from the location of the highest crest, which confirms the reliability of the proposed method even with moderately polluted measurements.

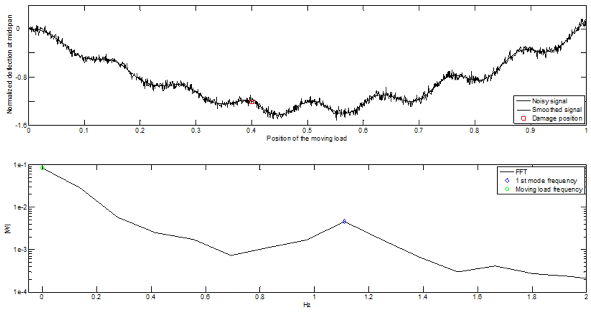


Figure 2: a) Forced response of the beam and b) its relative Fourier transform

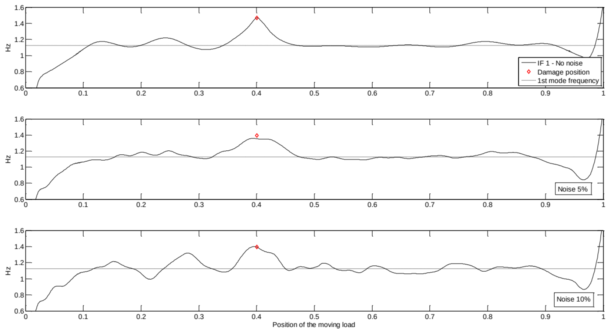


Figure 3: First IF curve with different levels of noise vs. length of the beam

The influence of the damage location in producing frequency modulation is considered: figure 4 shows the first IF obtained for three damage positions: 0.2L, 0.4L and 0.8L. It appears how the crest in the IF curve becomes higher and sharper as the damaged sections is closer to the end of the bridge.

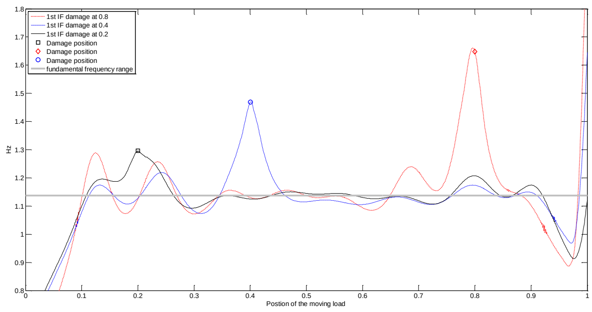


Figure 4: First IF curve for three damage positions on the beam

### 3.3.3 Time dependent systems

The determination of the load characteristics, namely the mass and velocity, is performed by an innovative optimization method, based on the use of EMD and HT, as explained ahead. To understand the basic principle of the proposed technique, it is worth to recall how the natural frequency $\omega_1(t)$ of an Euler-Bernoulli beam model changes with time, as a consequence of the moving mass. It is well established indeed that $\omega_1(t)$ can be approximated by the analytical formula:

$$\omega_1(t) = \frac{\omega_1}{\sqrt{1+\frac{2M}{\rho AL} sin\left(\frac{\pi Vt}{L}\right)}} \tag{1}$$

Equation (1) enlightens the functional relation between the fundamental frequency and the load characteristics. Both the mass and the speed of the moving load are estimated following a minimization error approach based on equation (1), once the left hand side is extracted from the measured dynamic response. The backbone of the method is articulated as follows:

a) data acquisition: the response $w(t)$ is measured by a single-point sensor placed at midspan;

b) data decomposition: $w(t)$ is decomposed into a family of IMFs through the EMD method;

c) data transformation: the instantaneous frequencies are evaluated with the application of HT to each IMF, the IF corresponding to $\omega_1(t)$, here identified $\tilde{\omega}_1(t)$, is selected;

d) data minimization: an error vector $\Xi = \{e_1, ..., e_{nt}\}$ is introduced, whose components are: $e_j(M,V) = \tilde{\omega}_1(t_j) - \omega_1(t_j),\ j = 1,..nt$,

where *nt* is the number of time samples. The load parameters, i.e. $\tilde{M}, \tilde{V}$, are estimated from the solution of the nonlinear least square minimization of the error function:

$\min_{M,V}\left\{\left\|\Xi(M,V)\right\|_2^2\right\}$, where $\|\ \|$ is for the norm of the vector.

Concerning point d), classical, derivative-based, optimization algorithms depend rather strongly on the initial guess, thus these techniques might only give a local solution. To skip this difficulty, a genetic algorithm (GA) is employed to solve the problem. We take advantage of the GA's benefits: they can quickly examine a large amount of data, and the choice of initial conditions does not affect negatively the outcome because they are discarded.

To evaluate the performance of the proposed technique for the estimation the load characteristics, a simple supported beam bridge, with the same characteristics of a Pescara bridge tested in [9], was considered, setting the load characteristic equal to M = 10 kg and V = 1 m/s [14]. Figure 5 shows the dynamic response of the system at midspan. The forced response can be considered as the sum of two harmonic waves controlled by the fundamental frequency $\omega_1$ and the loading frequency

$$\omega_v = V\sqrt[4]{\frac{\rho A}{EI}}\sqrt{\omega_1},$$

In this example they are 18.8 Hz and 0.17 Hz, respectively.

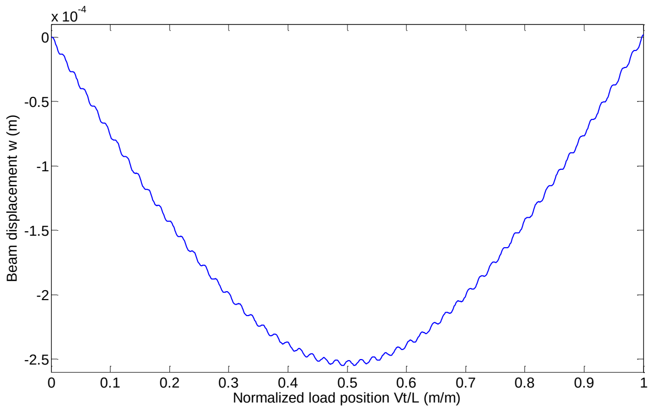


Figure 5: Dynamic response of the system at midspan

Figure 6 shows the Fourier transform of the dynamic response. Most of its energy is stored around the loading frequency. The spreading of energy around 18.8 Hz shows the frequency modulation induced by the load over the fundamental frequency. However the FFT is not suited to resolve the details of the phenomenon.

Figure 7 presents the estimated load characteristics, based on the previous data, after the use of the genetic algorithm formerly introduced. The estimated values are 10.6 kg and 1.05 m/s, with estimation errors of 6% and 5%, respectively.

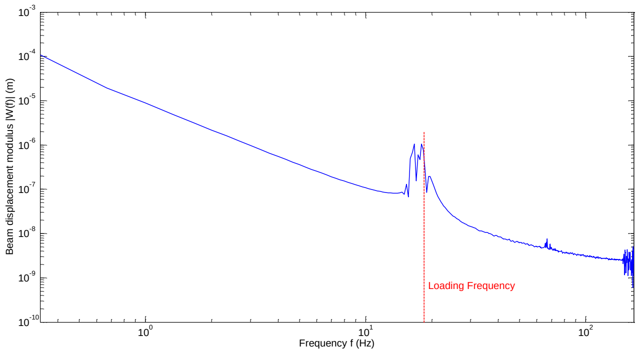


Figure 6: Fourier transform of the dynamic response

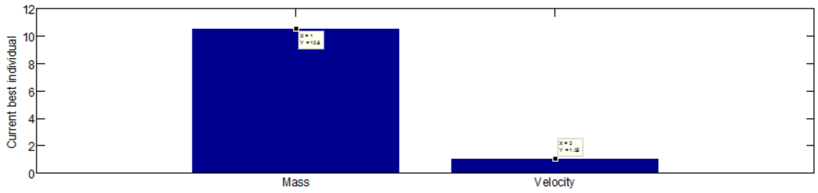


Figure 7: Estimated values of mass and speed

Figure 8 shows the fundamental frequency $f_{1NHT}$ evaluated with the NHT (Normalized Hilbert Transform) applied to the first IMF, compared to the analytical frequency $f_{1an}=\omega 1(t)\ /2\pi$, given by equation (1). Note that there is good agreement between $f_{1NHT}$ and $f_{1an}$ curves: $f_{1an}$ can be considered as the regression of $f_{1NHT}$ curve.

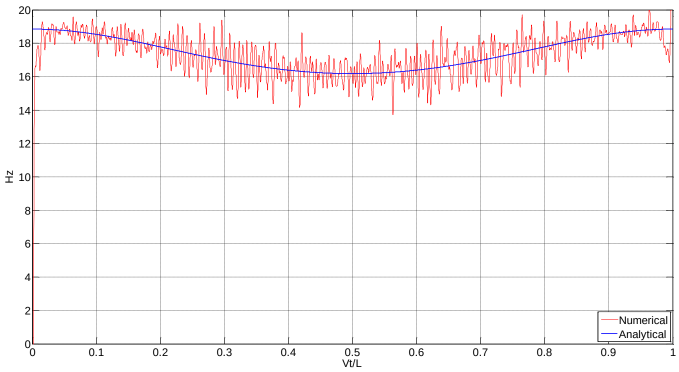


Figure 8: Comparison between $f_{1NHT}$ of the first implicit mode function and $f_{1an}$ (eq. (1)).

The damage location is estimated as follows [14]:

a) the $f_{1NHT}$ curve is smoothed using a moving average filter; the curve $f_{1S}$ is generated and the frequency modulations induced by both the moving mass and the damage are kept;

b) the estimated load characteristics are inserted into equation (1) and the fundamental frequency $\tilde{f}_1(t)$ is determined;

c) $\Delta f(t) = \left| f_{1S}(t) - \tilde{f}_1(t) \right| / \tilde{f}_1(t)$ is calculated; in this way the effect of the moving mass is filtered out and $\Delta f(t)$ retains only the frequency modulations induced by the damage;

d) the damage location is estimated by the time $t_d$ at which $\Delta f\left(t\right)$ reaches its maximum, by the formula $\tilde{L}_1 = \tilde{V} t_d$, as shown in the second subplot of figure 9. In the figure, $f_{1NHT}$, $\tilde{f}_1\left(t\right)$ and $\Delta f\left(t\right)$ are represented and the estimated location is $\tilde{L}_1 = 0.2045L$, with an estimation error about 2%.

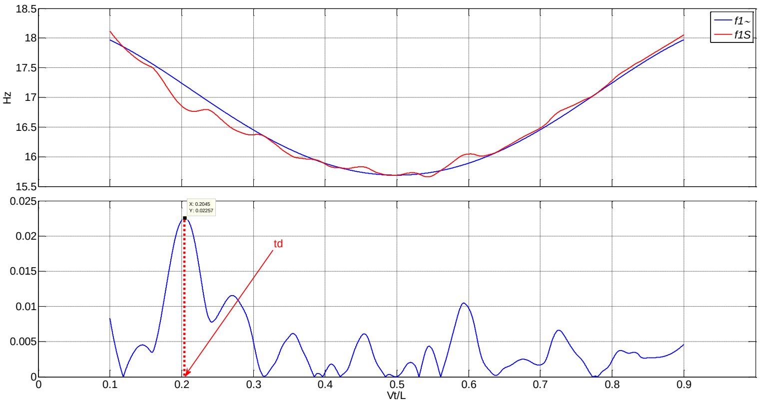


Figure 9: Estimate of the damage location

# 3 Train-Railway Monitoring

The train-railway monitoring is an important activity allowing for a variety of combination of algorithms and modelling. The Sapienza Team had the opportunity to collect a large amount of data, available for different processings, deterministic and stochastic as well, and introducing different models of the system under investigation. Moreover, as an additional interesting element, the monitoring goal includes two different subsystems: the railway and the train wheels, treating the data as a whole, indeed separating, by a suitable data processing, the diagnostic information for the railway and the train.

The data are obtained by a set of FBG sensors distributed along an experimentally equipped underground rail installed and active for more than two years.

More precisely, in this case, the desired goals can be summarized as follows:

- identification of railways system characteristics
  - detection of the rail roughness and wear
  - detection of railway local defects (work in progress)
- identification of the train wheels system
  - detection of wheel roughness and wear
  - detection of train load distribution
  - detection of train speed.

Not all these goals have been accomplished, and particularly the detection of the local damages on the rail is still investigated. In fact, following closely the lines presented in section 2, with some differences related to the infinite length of the rail with respect to the finite length of the bridge, it is possible to extend the Hilbert-Huang procedure to detect the railway local defects.

## 3.1 Sensor description and layout

The experimental set-up was installed between two stations in the subway of Milan. It is made of a set of FBG sensors to detect the strain deformation, static and dynamic, of the rail and the environmental temperature. A schematic description of the measurement chain is shown in figure 10, and consists in:

- a light beam signal, in the range of far infrared wavelenghts, generated by an optical led source; the light beam travels along an optical fiber equipped with FBG sensors attached to the rail;
- when the rail is deformed, the frequency bandwidth of the reflected light changes, and such variation is detected by a spectrum analyzer;

- the spectrum analyzer samples the analogical signal before sending it to the computer where the signal is suitably processed.

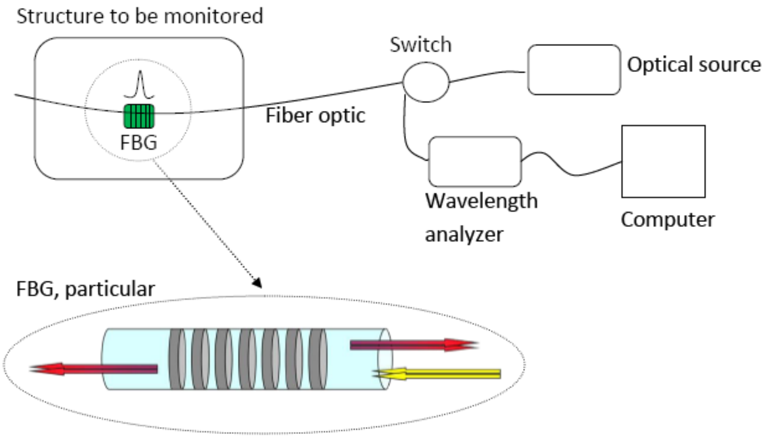


Figure 10: Sketch of the measurement chain

About 30 FBG sensors of strain and temperature are installed along the railway as illustrated in figure 11. The relative distance between a pair of sensors is within the range 10-20 m.

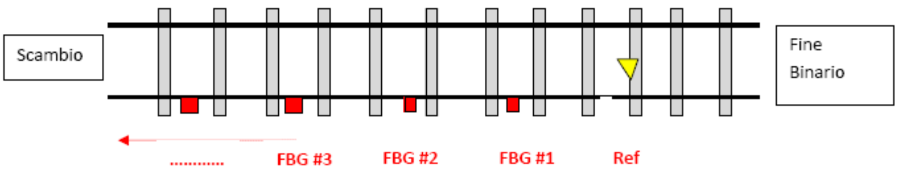


Figure 11: Experimental set-up

Figure 12 shows a detail of the optical sensor installed of the rail.

Figure 12: Installed FBG sensor

## 3.2 Detection of roughness and wear of rail and wheels.

In this case, the monitored system $S_m$ is limited to the acquired strain information acquired along the rail $\varepsilon(x_j,t)$. Indeed the interest here involves a rather large amount of unmonitored data $S_u$, specifically related to the roughness of the railway and the train wheels. To approach the problem, the definition of a response model of the system is crucial. In fact, the structural strain response $\varepsilon(x_j,t)$ of the railway is produced by the simultaneous presence of three excitation components: the moving load of the train along the rail, the wheels irregularity circular profile and the rail irregularity geometry. The mechanical model is determinant to understand the individual participation of these components to the measured response. Moreover, with the help of some restrictive but physically relevant hypotheses, it is possible to separate these components and their relative range of frequency, monitoring their respective levels that can be compared with some benchmark for the diagnostic process.

### 3.2.1 Modelling

The information used for the identification process comes from the dynamic equation of the rail. This allows to describe the rail excitation phenomena and obtain the main spectral characteristics of the acquired signal.

The rail can be modeled as a prototype structure consisting of an infinite beam on an elastic foundation excited by a set of lumped travelling masses, each carrying a portion of the train mass, considered integral to the wheels. The excitation is due to (i) the travelling load of the train, (ii) the vertical inertial loads due to the wheel-train mass, excited by the rail-wheels geometrical irregularities. With obvious meaning of symbols and considering now a single wheel, the system is described by:

$$EI\,\frac{\partial^4 w(x,t)}{\partial x^4}+[\rho A+m\delta(x-Vt)]\frac{\partial^2 w(x,t)}{\partial t^2}+\chi\, w(x,t)=mg\,\delta(x-Vt)+ma_w(t)\delta(x-Vt)$$

where $\chi$ is the stiffness of the elastic foundation and the last term on the right hand side accounts for the vertical acceleration of the train mass m due to the combined random irregularities at a single wheel-rail contact, i.e. a single wheel of the wagon. Therefore:

$$a_w(t)=\frac{d^2}{dt^2}\left[\, r(t)+h(t)\,\right]=\frac{d^2}{dt^2}\left[\, r(\vartheta)\big|_{\vartheta=\Omega t}+h(x)\big|_{x=Vt}\,\right]$$

where *r(θ)* and *h(x)* are two random signals. More precisely, the first is related to the wheel geometrical imperfections that make *r(θ)* random-periodic. The randomness is caused by the set of train wheels (of a wagon) that excites the rail, and each of the wheel signals can be considered as a sample of the same random process. The period is controlled by the wheel angular speed **Ω** and wheel radius *R*. The signal *h(x)*, related to the rail roughness, is simply random.

The form of the motion equation suggests two different types of rail responses: the first one is related to the load $mg\,\delta(x-Vt)$ for which the response can be found in the form $\Phi_{mg}(x-Vt)=\Phi_{mg}(\xi)$. Therefore, substituting into the equation of motion one obtains:

$$EI\,\Phi_{mg}^{iv}(\xi)+V^2\left[\rho A+m\delta(\xi)\right]\Phi_{mg}''(\xi)+\chi\,\Phi_{mg}(\xi)=mg\,\delta(\xi)$$

This equation can be analytically solved considering two solutions: one for positive $\xi$, the second for negative $\xi$, and imposing, for the two solutions, congruence conditions at $\xi=0$. For the purpose of this analysis, we are only interested here to the frequency content of the signals acquired by the sensors.

This analysis can be carried out only by using the dispersion relationship associated to the propagation problem. To this aim, the point $\xi=0$ is skipped, and the dispersion relationship is found looking for a solution of the form $e^{k\xi}$, leading to the dispersion relationship:

$$EI\,k^4+\rho AV^2k^2+\chi=0$$

Using general parameters found in the literature for underground railways (MKS units: $EI=3.7\cdot10^6$, $\rho A=50$, $\chi=5\cdot10^7$ ), this equation can be solved in terms of $k$ for different values of the train speed $V$. This implies that the solution is controlled by the factor $e^{jkVt}$ characterized by a circular frequency $\omega=2\pi f=kV$. The result for three different train speeds is: $f=2.1Hz$ for $V=10m/s$, $f=4.3\ Hz$ for $V=20\ m/s$, $f=10.9\ Hz$ for $V=50m/s$.

The second part of the excitation is more complex. In fact, simple travelling solutions are not admitted, because the wheel excitation is of the form $ma_w(t)\delta(x-Vt)$, that contains the time-dependent function $a_w(t)$. However, as a general consideration, the term $a_w(t)$ can be reduced to a suitable superposition of time-harmonic functions:

$$\sum_{n=1}^{N} C_n e^{j\omega_n t}$$

and therefore :

$$ma_w(t)\delta(x-Vt) = m\delta(x-Vt)\sum_{n=1}^{N} C_n e^{j\omega_n t}$$

This expression allows to look for solutions of the form

$$w(x,t) = \Phi_{ma_w}(x-Vt)\sum_{n=1}^{N} W_n e^{j\omega_n t} = \Phi_{ma_w}(\xi)\sum_{n=1}^{N} W_n e^{j\omega_n t}$$

It reveals that the rail response to the random loads comes from the product of two different factors. The frequency content response of the first term $\Phi_{ma_w}(x-Vt)$ can be evaluated using the dispersion relationship, while the second one can be derived directly inspecting the harmonic components $\omega_n$.

By substituting $\Phi_{ma_w}(\xi)\sum_{n=1}^{N} W_n e^{j\omega_n t}$ into the equation of motion, after some mathematics, we have :

$$EI\,\Phi_{ma_w}^{iv}(\xi) + \rho A\left[V^2\Phi_{ma_w}^{''}(\xi) - 2j\omega_n V\Phi_{ma_w}^{'}(\xi) - \omega_n^2\Phi_{ma_w}(\xi)\right] + \chi\,\Phi_{ma_w}(\xi) = 0$$

Again, the point $\xi=0$ is skipped, and the dispersion relationship is found looking for solution of the form $e^{jk\xi}$, leading to the dispersion relationship:

$$EIk^4 - \rho Ak^2V^2 + 2\rho A\omega_n kV + \chi - \rho A\omega_n^2 = 0$$

This equation must be solved in terms of k, varying both the train speed and the harmonic content of the signal (wheel and rail) here represented by $\omega_n$. Note that the rail and wheel signal components must be treated differently (see [15]), in that the wheel signal is periodic, so that a direct Fourier series representation with random coefficients can be used, while for the rail a continuous spectral representation must be used.

On the basis of developments presented in [15], the three frequency bandwidths related to the loads $mg\delta(x-Vt)$, $m\ddot{r}(t)\delta(x-Vt)$, $m\ddot{h}(t)\delta(x-Vt)$ can be determined. They are presented in table 1 for the three values of the speed V considered above.

| LOAD | BANDWIDTH | V=10m/s | V=20m/s | V=50m/s |
|---|---|---|---|---|
| $mg\delta(x-Vt)$<br>**Train load** | $\left[0, k^{(mg)}V\right]$<br>*k from equation (1)* | 0-2.1 Hz | 0-4.4 Hz | 0-10.9 Hz |
| $m\ddot{r}(t)\delta(x-Vt)$<br>**Random-wheel** | $\left[k_{\min}^{(wheel)}V, \omega_{\max}^{(wheel)} + k_{\max}^{(wheel)}V\right]$<br>*k from equation (2)* | 2.1-503 Hz | 3.9-1015 Hz | 17-2561 Hz |
| $m\ddot{h}(t)\delta(x-Vt)$<br>**Random-rail** | $\left[k_{\min}^{(rail)}V, \omega_{\max}^{(rail)} + k_{\max}^{(rail)}V\right]$<br>*k from equation (2)* | 2.2-52 Hz | 4.4-104 Hz | 11-267 Hz |

Table 1 : Spectra of the different load components

Such results show the following characteristics of the spectra:

(i) the train load spectrum develops in a low frequency range with respect to the others. However, a certain overlap is observed with the lowest frequency components of both the random-periodic wheel and random rail loads;
(ii) the two random loads overlap even if a much wider frequency spectrum characterizes the random-periodic wheel load;
(iii) the faster is the train, the lower is the overlap between train load and random loads.

A first consideration is that a simple frequency filtering of the data cannot separate the three contributions. This means that additional data processing must be used, manipulating suitably the data both in the time and frequency domains, and using statistical properties of the random data. More precisely, the separation of the train load from the random load is operated by the following operations: (i) high-pass filter in the frequency domain, (ii) chopping the data in the time domain.

Once the random load contribution is separated, the splitting of the wheel and rail components is made by following the procedure ahead:
(i) a covariance matris is constructed, organized by row and columns, associated respectively to wheels and measurement stations;
(ii) assuming stochastic independency of cross signals along this matrix, and between random-rail and random-wheel processes, it is possible to extract, from this matrix, two coupled equations where the unknowns are the power indexes related to the rail and wheels conditions, respectively. The solution of these equations provides an indication on the wear of the different wheels of a wagon (train) and of the different tracks of the rail, in correspondence to the measurement stations (see [15]).

The typical strain time history acquired by a FBG sensor when a six-car passenger train crosses a measurement station is shown in figure 13. The 24 axles are clearly indicated by the peaks in the signal, the highest strain peak is roughly 45 με: given the axle spacing the evaluation of the train speed is straightforward. The deformation of the rail depends on the train speed and weight as well as on the maintenance conditions of rail and wheels.

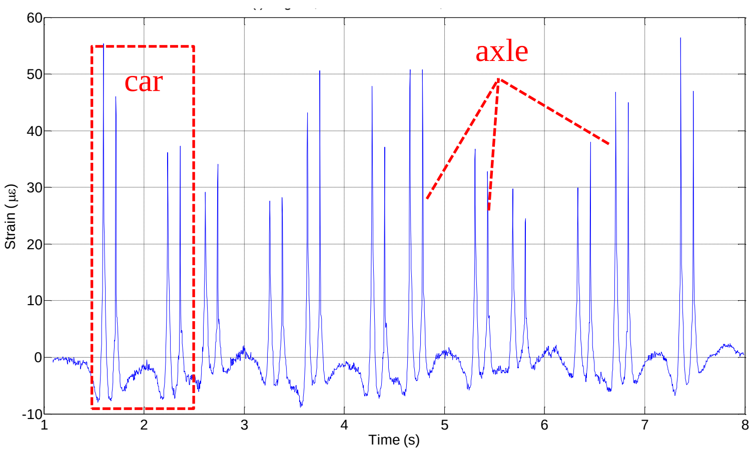


Figure 13: Strain time history when a six car passenger crosses a measurement station

In order to obtain an index concerning the condition of the wheels and the rail, the signal is normalized with respect to the mean values of the peaks, depending on the train load, and with respect to the train speed. The first subplot in figure 14 shows the normalized high-pass filter of the strain signal: the sharp peaks point out that the influence of the axles load is not completely removed by the filter. The second subplot in figure 14 shows the portions of the high-frequency signal obtained by chopping the data from a single boogie (within two consecutive peaks) form the signal: these zones are mildly affected by the train load.

Using the filtered and chopped signal (second subplot in figure 14), the power of the signal is computed:

$$\left\langle \varepsilon_c^{FC\,2}\left(x_i,t\right)\right\rangle = \frac{1}{n}\sum_{j=1}^{n}\left(\varepsilon_c^{FC\,2}\left(x_i,t_j\right)\right)^2 = E_{ci}^{(rail)2} + E_{ci}^{(wheel)2}$$

where the subscripts c and k relate to the car and FBG station, respectively, and n is the number of time steps of the signal for the c-th car. Note that $\varepsilon_c^{FC}(x_i,t)$ represent the strain response as a superposition of two independent effects: the first $E_{ci}^{(rail)}$ is the response of perfectly circular wheels rolling on a rough rail, the second $E_{ci}^{(wheel)}$ is the response of a flat rail when irregular wheels roll on it. For this reason we assume that $E_{ci}^{(rail)\,2} = E_i^{(rail)\,2}$ is independent of the car index c. Similarly we assume that $E_{ci}^{(wheel)\,2} = E_c^{(wheel)\,2}$ independent of the station index i.

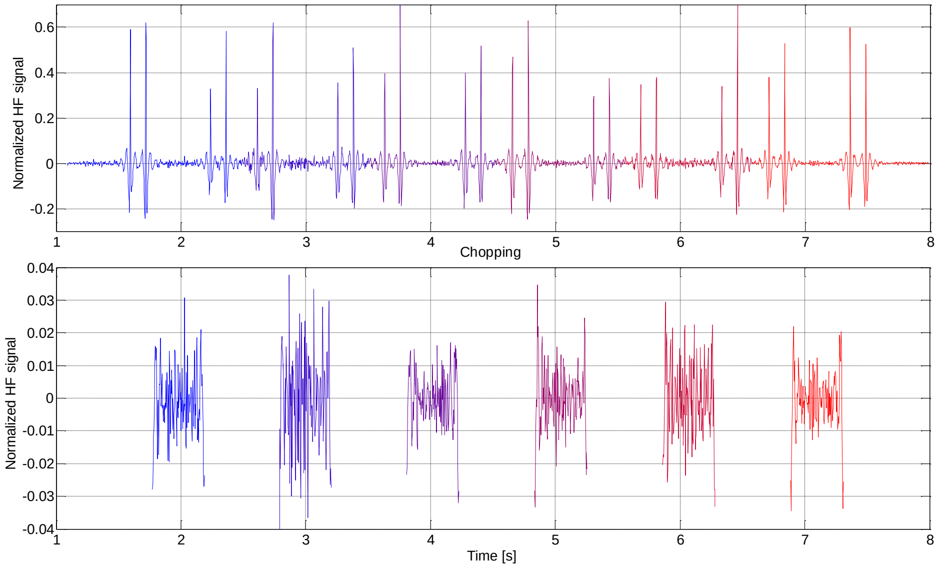

Figure 14: Filter and chopping operation on the strain signal

Using the compact notation:

$$R_i = E_i^{(rail)\,2}$$

$$W_c = E_c^{(wheel)\,2}$$

Figure 15 shows the rail index $R_i$ for 110 different train passages.

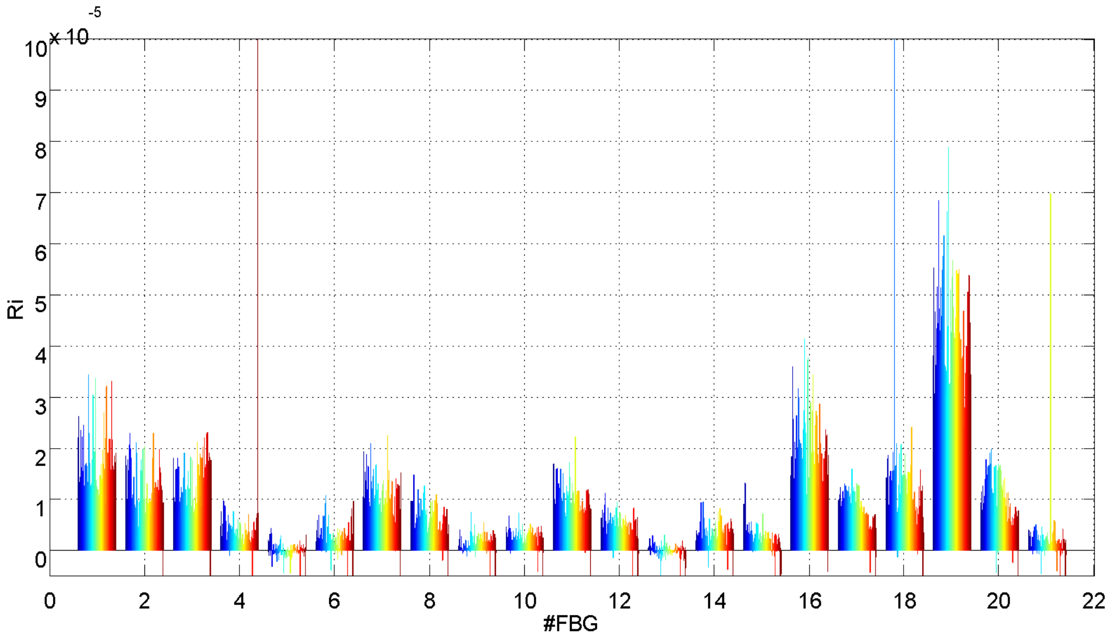


Figure 15: Ri index vs FBG stations. The bar colours identify different train passages.

It shows that:

- the rail around the 19th FBG station is in the worst condition in that it has the highest index, far greater than the others;
- the rail segments around the 5th, 9th and 13th FBG stations are in the best conditions;
- the regions of the rail around the 16th, 1st, 2nd and 3rd are also in pretty bad conditions;
- the variability shown by the different bars along the same FBG station is mainly due to the interaction of different wheels with the same part of the rail, which is not a completely independent random process.

Similar considerations can be made for figure 16 showing the wheel index $W_c$ :

- bars of the same colour provide information regarding the status of the wheels of the cars for the same train;
- the average damage is higher for the wheels of the 2nd and the 5th cars, roughly double than the others. This can be correlated with the average car load, which shows the 2nd and the 5th cars have the smallest load. This rather counter-intuitive result may arise from two effects:
    - vibrations induced by the wheel - rail contact are probably higher in light cars, that have a higher resonant frequency of the suspensions, somehow tuned with the typical wavelength of the wheel irregularities;
    - due to higher vibrations and lighter car load, the wheels may frequently lose the contact with the rail track, giving rise to shocks along the contact patch.

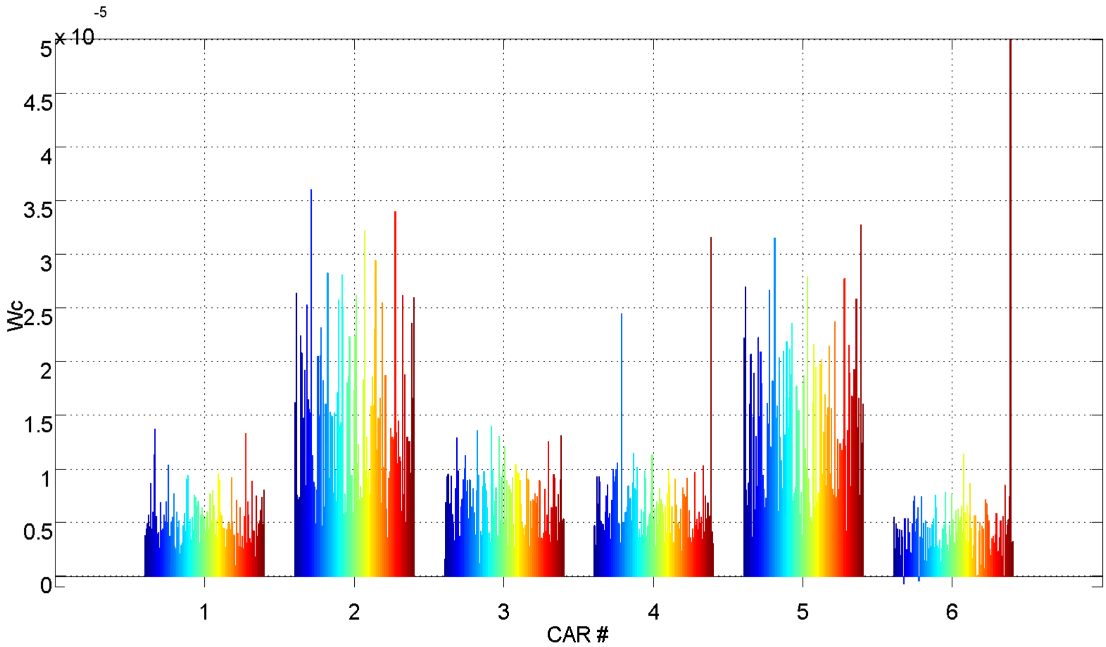


Figure 16: $W_c$ index *vs* wagon wheels. Bar colours show different train passages

# 4 Rolling tire stress and grip monitoring

This project is focused on the development of a new system for the real-time identification of the tire stress during rolling and residual grip estimation.

In this context three different goals and relative lines of research are in progress.

- Identification of the tire-road contact conditions (grip).
- Development of an appropriate sensor technology.
- Use of the grip information to control the electronic assisted drive devices.

The first line of research is thus based on the use of combined strain/vibration information inside the tire, from which relevant kinematic characteristics of the tire-road contact can be extracted, namely by a factor named area slip ratio. This process forms the basis of a new technology for grip identification, that also leaded to develop a new model of tire dynamics. The model permits to determine closed form analytical relationships between the measured strain/vibration data and the area slip ratio.

This approach is different from others developed in similar industrial research projects. In fact, the most advances technologies for grip identification are based on the use of MEMS that measure the acceleration at some points of the tire inner structure. The different choice of measurement strategies, acceleration versus strain, has a series of deep implications in terms of sensors, models and algorithms employed, and at the end outlines two completely different technologies of grip identification.

In this paper we summarize the model and the methodology described in [16] and some insights into the new approach of grip identification are outlined.

A first point that must be underlined is that a large number of mathematical models for tires exist in the technical literature (e.g. [17-21]). However, most of them are finalized to be used in the context of vehicles dynamic modeling, where the main goal is to determine the forces at the tire-road contact when the kinematic parameters of the vehicle and the tire are known. More precisely, in that context, one is interested in determining the longitudinal and lateral forces the tire generates when subjected to specified rolling conditions, characterized by longitudinal slip and slip angle, indeed kinematic parameters. However, the problem of the grip identification has a completely different goal. For this reason, the traditional models used for tires do not help much in the investigation of the tire grip, where the problem is to correlate some quantity measured inside the tire, strain or acceleration, to the phenomenon of adhesion between the rubber and the road.

A second important point is related to the need of defining preliminarily the goal of the grip identification. In fact, a unique definition of grip does not exist, and it is indeed important to define what is the goal of the identification process we desire. The tire grip is a complex phenomenon that occurs at the tire-road contact that is difficult to characterize and is controlled by a large number of parameters. Frequently, an elemental description of the adhesion phenomenon is made by the definition of the static and dynamic friction coefficients, that could be themselves the goal of the identification algorithm. This approach is skipped in [16], considering that these parameters are ultimately related to an attempt of force identification that is well known to be intrinsically ill conditioned. Therefore, one can reasonably expect that a force-based identification process has not robustness characteristics. In [16], the preferred strategy consists in identifying the kinematic conditions at the tire-road interface, without any direct involvement of force considerations. To illustrate this point, a brief description of the tire-road contact phenomenology is useful.

The wheel, as illustrated in figure 17, can be modeled as composed by two parts: one is a rigid body B (the rim), subjected to torque driving and braking actions; the other is the tire E, that wraps the first one, elastically deformable, both in the normal as well as in the tangential directions, $\eta$ and $\xi$ respectively. In [16], E is modeled through the coupling of a brush model attached to a rod-beam structure (brush-rod-beam BRB model). The contact patch develops along the $\xi$ axis for a total length $2c$. The peripheral part of the wheel is made of points the speed of which consists of four components: two are related to the rigid body motion of B, namely those related to its rotation and translation velocity, and two to the elastic motion of E, that involves normal and tangential speeds due to the elastic deformation of E. As a consequence of this complex speed composition, the peripheral points of the wheel along the contact patch are divided into two sets: points with zero relative speed with respect to the road, and points having non-zero relative speed. In figure 17, the first belong to the yellow segment of the contact patch, the second belong to the blue one. The model presented in [16] is addressed to identify the point $\xi^*$ along the contact patch, that marks the transition between the slip and non-slip region (blue and yellow, respectively), that clearly specifies the goal of the grip identification process. The ratio $\xi^*/2c$ is called area slip ratio, and provides a good indicator of the kinematic grip condition along the contact patch.

Note that this parameter provides a significant and relevant knowledge about the grip condition of the tire. In fact, when the slip-region expands along the contact patch over certain geometrical limits, or at a fast speed, these are indicators that the tire is going toward a dangerous grip condition. The conditions in which $\xi^*$ collapses in the two extreme and opposite points of the contact segment, the trailing edge and the leading edge, characterized by $\xi^*/2c=-0.5$ and $\xi^*/2c=0.5$ , respectively, are associated to the extreme conditions of a complete macroscopic slip of the wheel, and of complete grip, respectively.

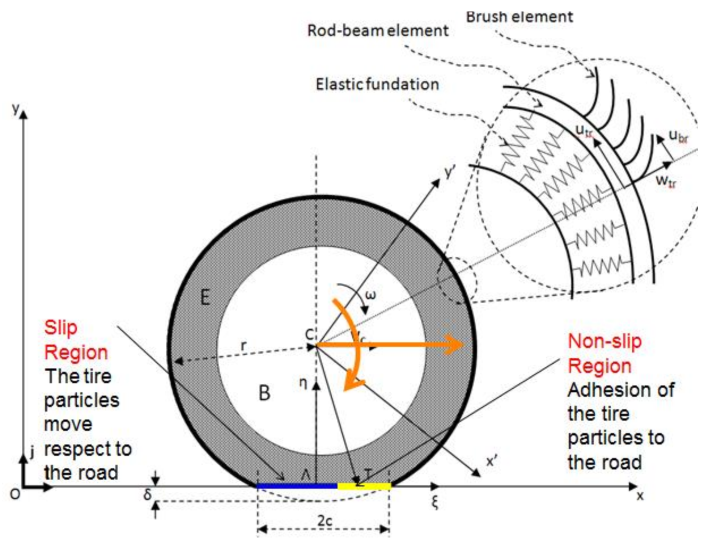


Figure 17: Scheme of the BRB model of the tire

On this basis, a suitable algorithm can extract the contact kinematic parameters from the time history of the internal strain of the rolling tire. Therefore, the goal of the identification process can be simply summarized and formalized as follows:

$$\xi^* = F\,[\varepsilon(\tau)], \quad \tau \in \left[0, \frac{2c}{\omega R}\right]$$

where $\varepsilon$ is the strain measured by the sensor introduced inside the tire, that scans the contact patch during the time interval $2c/\omega R$. The model developed in [16], provides the structure of the functional relationship F between $\xi^*$ and $\varepsilon$. More precisely, the authors show how the presence of a discontinuity in the kinematic contact conditions affects the signal $\varepsilon(t)$. In other words, the algorithm is aimed at identifying $\xi^*$ in terms of a weak discontinuity characteristic of the strain measurement, produced by the transition of the slip conditions at the tire-road interface. In this case the monitored system $S_m$ is known through the measured $\varepsilon(t)$, while the unmeasured part $S_u$ is simply identified by $\xi^*(t)$.

An example of experimental strain measurement is shown in figure 18, acquired during an acceleration

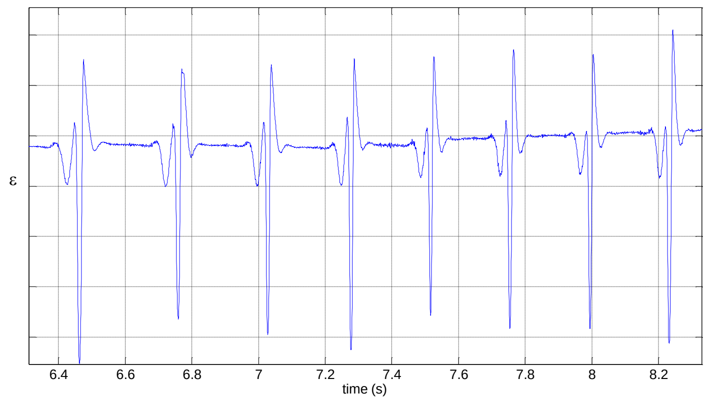


Figure 18: Experimental strain measurement, acquired during the acceleration of the vehicle

transient of the vehicle front wheel. It appears that the sequence of peaks is related to the rotation process (one peak per round), and the frequency of the peaks increases as the speed increases, while the maximum amplitude of the signal decreases because of the load transfer to the rear wheels produced by the acceleration.

As shown in figure 19 the algorithm takes information, for each round of the wheel, only from the portions of the signal corresponding to the scanning of the contact patch (red bullet in figure 19). This portion provides the distribution of the strain along the contact patch, as shown in figure 19. This zoom operation shows also that a series of ripples characterizes the *ε(t)* signal, along the contact patch due to the tire vibrations and to the intrinsic measurement noise. However, the use of some algorithms as the one described in [16], permits to determine the most probable collocation of the discontinuity of *ε(t)* along the contact patch, identifying $\xi^*$ as it is shown in figure 19.

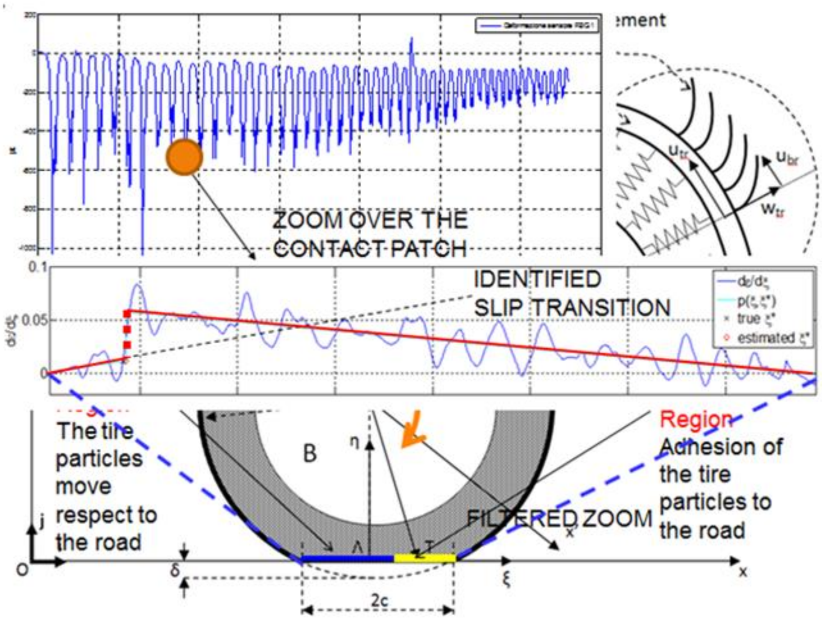


Figure 19: Scheme of the slip-grip identification algorithm

Both numerical simulations and a first set of experiments show that this technique is an appealing and powerful tool for grip identification.

The main points (goals) of this part of research can be summarized below:

i) identify the grip characteristics involving only strain-based information;

ii) the tire-road grip is determined on the basis of kinematic considerations only, namely determining the fraction of contact area where a slip condition holds. This geometric-kinematic parameter, named area slip ratio, skips potential problems related to the grip analysis based on force identification, that is indeed well known to be ill-conditioned inverse problem;

iii) considerations (i) and (ii) show that the method uses a direct correlation between slip kinematic conditions, involving only the tire velocity field on the contact area and the strain. The strain data contains space derivatives, avoiding the problem of calculating them by finite difference procedures operated by single-point-sensors, as for the accelerometers, making the data process much more robust and permitting a useful integration of acceleration (vibration) data;

iv) the developed theoretical model is aimed at correlating in the simplest manner the strain information and the contact kinematics. The model is able to determine analytically this correlation. The model permits to compare the theoretical model with the measured strain time-history extracting the desired parameters, effectively filtering the data noise effects.

A second line of tire research is the result of a new patent (A. Carcaterra, N. Roveri, M. Platini), that is not possible to comment here explicitly being it still the subjected of the patenting process. The strain sensors inside the tire and related data for the real-time identification of the residual grip on each tire of the vehicle are processed on board. The experimental setup and preliminary tests are in progress on the prototype vehicle HU245, figures 20 and 21. The system is equipped with a set of more than 20 strain sensors inside the tire that transmit the signals out of the tire by special joints. The identification grip algorithm previously described is applied to the acquired data.

The third line is devoted to the use of the grip information extracted from the apparatus previously described. In particular the unit uses the grip distribution among the wheels to distribute properly the braking torque in a fashion that maximizes the overall vehicle braking space.

Figure 20: The grip monitoring system mounted on the wheel of the test car HU245

Figure 21: The grip monitoring system mounted on the test car HU245

# 5 A new measurement device for air speed estimation

The measurement of fluid speed is a problem of practical importance. In the technical literature and at the actual state of the art, many methodologies exist to perform such a measurement. The Pitot tube represents the most widespread and well known instrument for fluid speed. The hot wire anemometry-HWA is also a well-known technique, based on the capability of the fluid flow to remove heat produced by an electric current on a conductive wire, regulating in this way its temperature and electrical resistance that can be measured. More recently, the particle image velocimetry PIV, has gained a great importance both in scientific investigations as well as in engineering applications, and can rely on the most recent advances in the fields of optics, high speed video cameras, informatics and signal processing, allowing to follow the velocity field in a monitored section of a fluid flow. Moreover, in more recent times, it is also available a three-dimensional version of the PIV, named 3C-PIV (three components PIV) that is indeed capable of monitoring three-dimensional velocity fields characterized by large out-of-plane velocity components.

In this paper, a new system is presented that the authors name cold wire anemometry-CWA that is based on the use of an optical fiber equipped by FBG sensors directly exposed to a fluid flow. In the following a brief summary of its working principle and some preliminary results are illustrated.

An optical wire mechanically consists of an elastic cable that, when subjected to transverse loads (orthogonal to the wire axis), reacts by modifying its shape following the elastic catenary configuration and, as a consequence, an axial stress is generated along the wire. Therefore, an optical wire exposed to the action of a fluid flow, the velocity of which is orthogonal to the wire axis, produces an axial stress along the optical wire. If this is equipped by FBG sensors, they reveal the amount of stress generated. If a suitable model of the wire mechanical response is available, one can determine the aerodynamic transverse load. Finally, based on an aerodynamic drag model, a correlation between aerodynamic loads and the fluid speed can be determined and, as a final result, one can correlate the measured axial stress of the wire to the fluid speed.

In this identification process the sensor is the optical wire with its mechanical characteristics (length, section, Young modulus) and the embedded FBG sensors. The algorithm of speed identification is based on two coupled models: one describing the cable mechanical response of the wire, the second the aerodynamic load. However, the relationship between the measured strain and fluid speed is rather complicated.

Let us consider an optical wire (Young modulus $E$, cross section area $A_0$ ) of length $l$ at rest that, under a given pre-stress load, becomes of length $L$, the distance between the end points of the wire during the measurement. At one of the fixed end points, one has the axial and the normal reactions with respect to the wire axis (of abscissa $s$), $H$ and $R$, respectively. The fluid flow is assumed to have only a normal velocity component $V(s)$ with respect to the wire axis. The fluid loads the wire through a force $Q$, that depends on the local Reynolds number $\mathcal{Re}$, and on $V^2$ through the drag coefficient $C_D$. With these assumptions, the mathematical model of the problem relies on the set of equations:

$$\begin{cases} T(s) = \sqrt{H^2 - [R - Q(s)]^2} \\ \int_0^L [R - Q(\xi)] \left[ \frac{1}{EA_0} + \frac{1}{T(\xi)} \right] d\xi = 0 \\ H\left[ \frac{L}{EA_0} + \int_0^L \frac{d\xi}{T(\xi)} \right] = l \\ Q(s) = \frac{1}{2} \rho d \int_0^s V^2(\xi) C_D [\mathcal{Re}\{V(\xi)\}] d\xi \end{cases}$$

This represents a nonlinear integral-algebraic equations system. The two quantities that would be correlated are $V(s)$ and $T(s)=EA_0\,\varepsilon(s)$, where the strain $\varepsilon$ would be known, at least at some points, through the FBG measurement. Therefore, the written system of equations, could produce $V$ once $T$ is known (or viceversa), where the set of unknown are $V$, $Q$, $R$, $H$, and four equations are available.

The method to identify the fluid speed is based on two different approaches. The first is to use the illustrated mathematical coupled model to generate numerically the speed-strain correlation curves; the second is to use calibration experiments, that directly measure the strain through the FBG sensors, and through an independent measurement system, e.g. a Pitot tube, determine the related speed.

Figure 22 shows the correlation determined by the simulations through the previous set of equations.

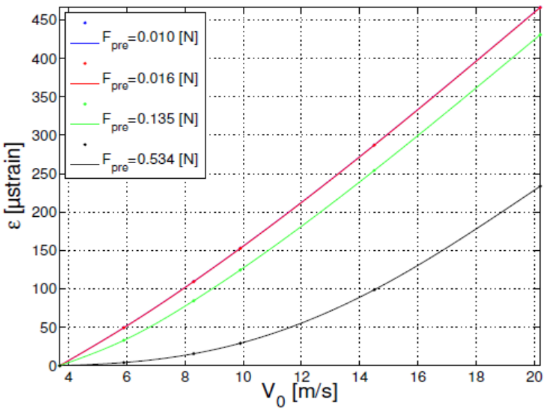


Figure 22: Strain vs air speed, for different values of wire pre-stress

The fluid velocity profile along the wire is assumed to be constant. The equations are solved for different values of $V$ and $T(s)$ is determined numerically. However, its value does not change sensibly along the wire span, and even a single FBG would be sufficient in this case to identify the strain along the whole cable. On the vertical axis of figure 22 the sensor measurement is represented for different values used for the air speed (represented on the horizontal axis). Moreover, different curves are obtained by varying the pre-stress of the wire, that is the ratio $L/l$. It appears that the anemometer sensitivity is higher for lower values of the wire pre-stress.

Figure 23 shows the comparison between experimental data and simulated data in the wind tunnel, where it appears the model used for the identification of the air-speed and experiments are in good agreement.

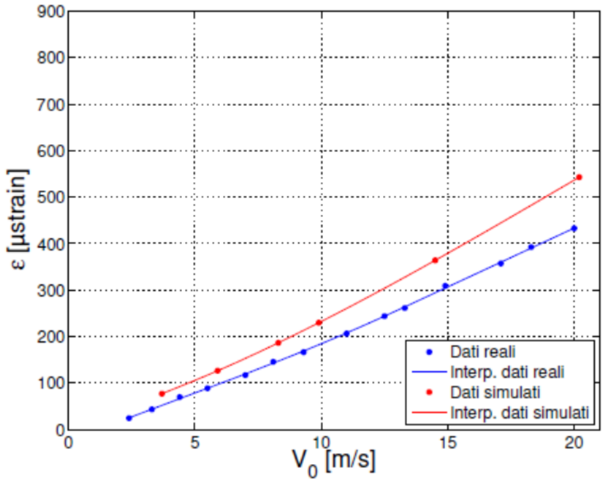


Figure 23: Comparison between experimental (Pitot) and simulated data

This preliminary analysis of the air speed measurement system outlines a potential opto-mechanical technology for the identification of fluid flow characteristics. It appears clearly, from the written equations, how the air speed measurement belongs, in this view, to an identification process that passes through the modeling of a coupled opto-aeroelastic problem, where $\mathbf{S}_m$ is known through the measured $\varepsilon(t)$, while the unmeasured part $\mathbf{S}_u$ is $V(t)$. Figure 24 shows the experimental set-up and the test in the wind gallery.

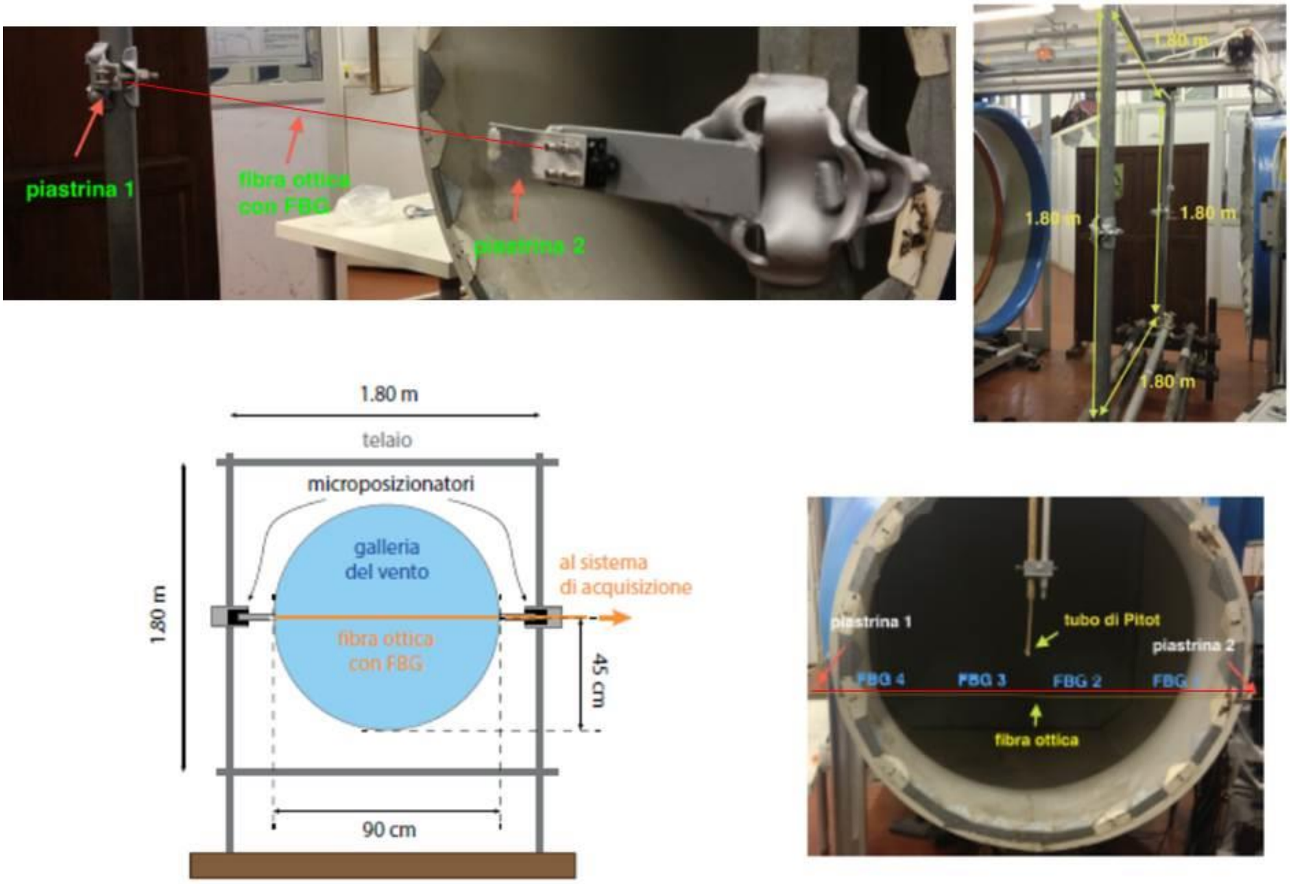


Figure 24: Experimental set-up in the wind gallery

# 6 Concluding remarks

This paper presents a review of researches developed at the University La Sapienza, Roma, aimed at showing new technologies related to the application of FBG sensors and to health monitoring of civil and mechanical systems. Particularly the focus is here addressed to (i) the detection of local defects of bridges, (ii) identification of railways and train wheel characteristics, (iii) monitoring of tire stresses and grip conditions, (iv) development of a new measurement device for air speed estimation, but other significant applications are taking advantage of these works, as those in progress related to the shape monitoring of sailing boat musts and airplane wings for performance optimization, and the control of high speed boat drones and engines for diagnostic purposes.

The paper is framed in the context of a monitoring technology, including an identification goal, the use of appropriate sensors, the development of a targeted model and an identification algorithm which represents the final processing to reach the expected goal. Most of the applications considered in this paper use FBG sensors, that seem particularly convenient at least in cases when the range of frequency is not too high.

The models developed for the detection of local defects on bridges and viaducts, for the characterization of rail and wheels characteristics, as well the one used for the monitoring of the tire grip are totally dedicated to the particular applications considered and are definitely promising for future developments. So far they were very useful to give important indication on the processing of experimental data to reach the goal expected.

With reference to the applications presented in the paper, we wish to highlight the main results.

a. Local damage detection. The method, based on the EMD and HT, can work using a single measurement point and produce good identification results. It is quite robust and able to identify the load characteristics with good accuracy, generally larger than 90%. Once the load characteristics are estimated, the first natural frequency is analytically evaluated and subtracted to the empirical instantaneous frequency, computed via HT. A normalized distance function is generated, where the effect of the moving mass is filtered out. The location of the damage is estimated by the maximum of the distance function. The method is capable to identify moderately damaged sections, with crack depths larger than 25% of the section height. Results are not very sensitive to damage position and ambient noise. The speed of the moving load plays a fundamental role on the estimation process: as the velocity increases the EMD becomes unable to separate the frequency components of the signal, thus the proposed technique fails to identify the load characteristics and/or a potential damage.
b. Detection of rail and wheels roughness and wear. In order to accomplish with the goal, a set of FBG sensors are used along the railway. Since two different loads must be considered, together with the moving mass of the train, an appropriate model has been developed to check the respective frequency bandwidths of the separate loads and operate a suitable post-processing of the strain data, consisting in a high-pass filtering and chopping. In this way it is possible to define two different indexes related to the rail and wheels conditions that put in evidence the roughness conditions of each wheel and the portions of track, more damaged along the rail.
c. Tire-grip identification. The grip level can be identified using only a geometrical-kinematic parameter based on slip conditions along the contact region, skipping any interface-force related quantity and independently of the knowledge of any of the tire construction parameters. The data necessary to develop the procedure are only a set of strain measurements along the tire. A patented prototype system is now running on a real vehicle and the perspectives for predicting in advance the reach of a potential wheel blockage, before a complete slip of the wheel, are very realistic.
d. Measure device for air flow speed. The sensor developed uses an optical cable equipped with a set of FBG sensors and measures, under the air flow, the strain of a deformed optical wire. Though a set of physical equations, it is possible to relate the air speed to the stress of the wire. Experimental test are under development to highlight the efficiency of this sensor with respect a classical Pitot tube.

## References

[1] N.E. Huang, Z. Shen, S.R. Long, M.C. Wu, H.H. Shih, Q. Zheng, N. Yen, C.C. Tung, H.H. Liu, *The empirical mode decomposition and the Hilbert spectrum for nonlinear and non-stationary time series analysis*, Proc. R. Soc. London A 1998, vol. 454, 903–995.

[2] N. Roveri, A. Carcaterra, *Damage detection in structures under travelling load by Hilbert-Huang transform,* Mechanical Systems and Signal Processing, 2012, vol. 28,128-144.

[3] W. Fan, *Vibration-based Damage Identification Methods: A Review and Comparative Study*. Proc. Structural Health Monitoring, 2010, vol. 10, 83-111.

[4] J.N. Yang, P.C. Chang, H. Fujitani, H. Li, B.F. Spencer, Y.L. Xu, F.G. Yuan, *Structural control and health monitoring*, Proceedings of International Conference on Advances and New Challenges in Earthquake Engineering Research 2002, vol. 3, 9–14.

[5] L.W. Salvino, *Evaluation of structural response and damping using empirical mode analysis and HHT*, Fifth World Multiconference on Systemics, Cybernetics and Informatics, July 22–25, Orlando, FL, 2001.

[6] M. Abdel Wahab, G. De Roeck, *Effect of temperature on dynamic system parameters of a highway bridge.* Structural Engineering International 1997, vol. 4, 266–270.

[7] J. Chance, G.R. Tomlinson, K. Worden, *A simplified approach to the numerical and experimental modeling of the dynamics of a cracked beam*. Proc. 12th International Modal Analysis Conference, Honolulu, USA, 1994, 778–785.

[8] F. Dell'Isola, F. Vestroni, S. Vidoli, *Structural-damage detection by distributed piezoelectric transducers and tuned electric circuits*, Proc. Research in Nondestructive Evaluation 2005, vol. 16, 101-118.

[9] F. Vestroni, J. Ciambella, F. Dell'Isola, S. Vidoli, *Damage detection with auxiliary subsystems*, CIMTEC, Proceedings of 3rd International Conference on Smart Materials, Structures and Systems – Emboding Intelligence in Structures and Integrated Systems 56, 2008, 401-413.

[10] A. Bellino L. Garibaldi, S. Marchesiello, *Determination of moving load characteristics by output-only identification over the Pescara beams*, Journal of Physics: Conference Series, 2011, 301(1).

[11] H. Ouyang, *Moving-load dynamic problems: A tutorial (with a brief overview)*. Mechanical Systems and Signal Processing, 2011, vol. 25, 2039-2060.

[12] S. Zhong, S.O. Oyadiji, K. Worden, *Analytical predictions of natural frequencies of cracked simply supported beams with a stationary roving mass*. Journal of Sound and Vibration, 2008, vol. 311, 328–352.

[13] H. Bulut, O. Kelesoglu, *Comparing numerical methods for response of beams with moving mass.* Advances in Engineering Software, 2010, vol. 41, 976-980.

[14] N. Roveri, A. Carcaterra, *Unsupervised identificationof damage and load characteristics in time-varying systems.* Continuum Mechanics and Thermodynamics. In press,

[15] N. Roveri, A. Carcaterra, A. Sestieri, *Integrated system for SHM and wear estimation of railway infrastructures*, Proc. Surveillance7, 2013.

[16] N. Roveri, A. Carcaterra, *Tire grip identification based on strain information: Theory and simulations*, Mechanical Signal and Signal Processing, 2013, in press. (http://dx.doi.org/10.1016/j.ymsp.2013.06.002).

[17] H.B. Pacejka, *Tyre brush model*, Tyre and Vehicle Dynamics, Elsevier, Oxford, 2005, 93-134.

[18] A. Sorniotti, M. Velardocchia, *Enhanced tire brush model for vehicle dynamics simulation*, SAE Technical paper, 2008-01-0595.

[19] H.B. Pacejka, *Semi-empirical Tyre models*, Tyre and Vehicle Dynamics, Elsevier, Oxford, 2005, 156-215.

[20] H.B. Pacejka, *The tread simulation model*, Tyre and Vehicle Dynamics, Elsevier, Oxford, 2005, 134-147.

[21] H.B. Pacejka, *Non steady state out-of plane string-based tyre models*, Tyre and Vehicle Dynamics, Elsevier, Oxford, 2005, 216-294.